Brillouin light scattering on yttrium iron garnet films in a magnetostatic wave device structure

G. Srinivasan and C. E. Patton
Department of Physics, Colorado State University, Fort Collins, Colorado 80523

P. R. Emtage
Westinghouse Research and Development Center, Pittsburgh, Pennsylvania 15235

(Received 19 September 1986; accepted for publication 11 November 1986)

Brillouin light scattering (BLS) has been used for the direct detection of magnetostatic wave (MSW) excitations in a MSW microwave device structure. The results are for a signal-to-noise enhancer device which consists of a yttrium iron garnet (YIG) film on a gadolinium gallium garnet substrate. The YIG film is in contact with a 30-μm-wide stripline and the static magnetic field is parallel to the stripline. MSW excitations were observed over the frequency range 2–4 GHz. At low power, magnetostatic surface waves (MSSW) were excited with propagation perpendicular to the stripline and field direction. At high power, parametric half-frequency magnons were also observed. The measured magnon dispersion for the MSSW excitations, determined using the wave vector selective capabilities of the BLS spectrometer, is in good agreement with theory. The measured intensity profiles for MSW excitations at low-power levels show strong MSSW excitations over the entire surface wave band. At high power, the scattering intensity for surface MSW excitations saturates and is accompanied by a strong parametric magnon signal.

I. INTRODUCTION

The propagation characteristics of magnetostatic waves (MSW) in yttrium iron garnet (YIG) films have provided the physical basis for a number of microwave signal processing devices, including delay lines, filters, resonators, and signal-to-noise enhancers.[1] The theory of MSW excitations in magnetic films and their propagation characteristics were first studied by Damon and Eshbach.[2] Device design has generally relied on the theoretical properties of such waves, with recourse to empirical characterization only after the device is designed and constructed. With the Brillouin light scattering (BLS) technique, which is capable of measuring directly the dispersion and intensity of magnetic excitations, it is possible to measure the dispersion properties and energy flow profiles of MSW excitations *in situ* in actual device configurations.[3,4] Recent BLS studies on one such device, a signal-to-noise enhancer, are presented in this paper.

The main components of the signal-to-noise enhancer device are a YIG film on a gadolinium gallium garnet (GGG) substrate and a stripline conductor in contact with the garnet film.[5,6] A static field is applied parallel to the stripline axis. A microwave signal in the stripline excites magnetostatic surface waves (MSSW) in the YIG film, and this leads to attenuation of the stripline power. For input powers above some threshold level, the MSSW signal saturates due to spin wave instability processes[7] and the insertion loss of the stripline decreases. One has, in effect, a signal-to-noise enhancer.

In Brillouin light scattering, the interaction between the incident laser light and the magnetic excitations in the material results in frequency shifted scattered light. The Brillouin spectrum is obtained by analyzing the scattered light with a Fabry–Perot interferometer. The phenomena in the signal-to-noise enhancer device involve excitations of two types: (1) the magnetostatic surface waves which are excited directly by the stripline and (2) the parametric half-frequency spin waves which are pumped by the MSSW signals at high power. Both types have been studied by the BLS technique. Scattering due to MSSW magnons was observed in the BLS spectra at low powers. Parametric half-frequency spin waves were observed at high powers, in addition to the MSSW signals. It was possible to determine the in-plane propagation directions for both types of excitations. The light scattering data on the magnon dispersion for the MSSW have been found to be in good agreement with the theoretical dispersion for the Damon–Eshbach surface waves. The BLS data on intensity profiles for the magnetic excitations correlate nicely with microwave loss measurements on the device. Brief reports on these results have been published previously.[3,4]

In addition to the device implications of this study, one important accomplishment of basic importance has been the BLS observation of surface magnons in YIG films, per se. Even though thermal MSSW signals have been observed in thin film materials such as iron and nickel,[8] BLS studies have so far failed to resolve thermal MSSW excitations in YIG. The present data show that these surface modes *can* be observed in YIG, at least under conditions of external excitation.

II. MAGNETIC EXCITATIONS IN THIN FILMS

This section deals with the properties of the magnetic excitations which are important in the device structure, that is, the bulk spin waves and the surface waves mentioned above. (The terms "magnon," "spin wave," and "excitation" will be used somewhat interchangeably in this paper.) The situation for bulk and surface waves in the limit of no exchange is summarized in Fig. 1. For the bulk spin wave modes, the excitation profiles across the film thickness correspond to a set of standing waves. The bulk magnon fre-

 0021-8979/87/062318-09$02.40 © 1987 American Institute of Physics

Downloaded 26 Dec 2001 to 129.82.140.114. Redistribution subject to AIP license or copyright, see http://ojps.aip.org/japo/japcr.jsp

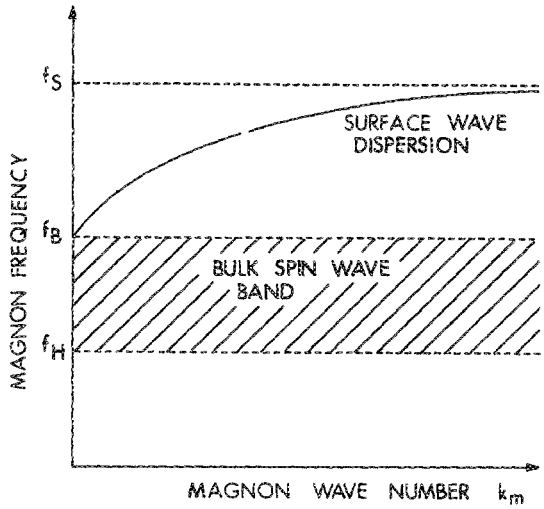

FIG. 1. Schematic diagram showing the bulk spin wave band and the frequency vs wavenumber dispersion for the magnetostatic surface wave with an in-plane wave vector which is perpendicular to the in-plane field. The frequencies f_H, f_B, and f_S represent the lower limit for bulk spin waves, the upper limit for bulk spin waves (and lower limit for the surface waves), and the upper limit for surface waves in in-plane magnetized slabs, respectively.

quency f_b, ignoring the effect of exchange, is given by

$$f_b = \gamma[H(H + 4\pi M_s \sin^2\theta_k)]^{1/2}, \quad (1)$$

where γ is a reduced gyromagnetic ratio, $4\pi M_s$ is the saturation induction, and θ_k is the propagation angle, i.e., the angle between the total magnon wave vector $\bar{k}_m$ and the static applied field $\bar{H}$. With γ in GHz/kOe, H in kOe, and $4\pi M_s$ in kG, f_b is in GHz. This convention will be followed throughout this paper.

The cross-hatched portion in Fig. 1 represents the frequency region for bulk, low k_m-value (no exchange) spin waves in the film. This bulk band is actually made up of a family of discrete magnetostatic wave (MSW) dispersion curves.[2] These bulk band MSW details are not central to the present results. The upper and lower frequency limits for these bulk spin waves are designated by f_B and f_H, respectively. From Eq. (1), propagation in a direction perpendicular to the static field ($\theta_k = 90°$) yields an expression for the upper limit,

$$f_B = \gamma[H(H + 4\pi M_s)]^{1/2}. \quad (2)$$

For parallel propagation ($\theta_k = 0°$), one obtains the lower bulk spin wave frequency limit,

$$f_H = \gamma H. \quad (3)$$

The f_B parameter also corresponds to the lower-frequency limit for surface magnons in the in-plane magnetized film.

The magnetostatic surface waves (MSSW) for in-plane magnetized slabs propagate in the slab plane. The surface character is related to the decay of the mode response into the slab interior from the surface with which that particular MSSW mode is associated. The propagation for MSSW excitations is not strictly bidirectional. For waves traveling perpendicular to the static field, for example, propagation for the waves associated with a given surface (e.g., a decay in amplitude away from that surface) is in one direction only; that direction is given by the cross product of the static field vector $\bar{H}$ and the outward surface normal. Of course, for any finite thickness slab, the MSSW mode associated with a given surface will have some residual amplitude at the opposite surface.

For propagation perpendicular to the applied field, the surface magnon frequency f_s is specified by[2]

$$f_s^2 = f_B^2 + (\gamma 2\pi M_s)^2(1 - e^{-2k_m d}), \quad (4)$$

where d is the film thickness and k_m is the surface magnon wave number. The k_m dependence of the surface magnon frequency for perpendicular propagation ($\bar{k}$ and $\bar{H}$ perpendicular) will be an important consideration for the coupling in the stripline device structure considered later. The dispersion relation of Eq. (4) is shown graphically in Fig. 1. The dispersion curve merges with the bulk spin wave band at f_B for $k_m = 0$. The upper limit frequency for surface modes f_S is simply

$$f_S = \gamma(H + 2\pi M_s). \quad (5)$$

This upper limit frequency for surface modes corresponds to the $k_m = \infty$ wavenumber limit.

The main point here is that f_B and f_S represent the frequency limits over which surface waves may be excited in the YIG film. The wavenumber for the excited MSSW signal which can be supported in the device ranges from a zero value at f_B to a large value at f_S. For excitation frequencies outside the f_B–f_S range, propagating MSSW signals can no longer be generated and the device ceases to operate. In microwave loss measurements on an actual device, the excitation of MSSW signals is manifested by a strong attenuation between the stripline input and output. The main objective of this study is to directly detect these magnetic excitations by the BLS technique.

III. THE MSW DEVICE

The signal-to-noise enhancer device structure is shown schematically in Fig. 2. The 1.8-cm-long and 26.6-μm-thick YIG film on a gadolinium gallium garnet substrate is in contact with a 30-μm-wide stripline on an alumina ground plane. As discussed above, the type of wave which can be supported in the YIG film is controlled by the magnitude and direction of the applied field $\bar{H}$. With $\bar{H}$ parallel to the stripline, as in Fig. 2, the microwave power can excite magnetostatic surface waves in the YIG film which carry power

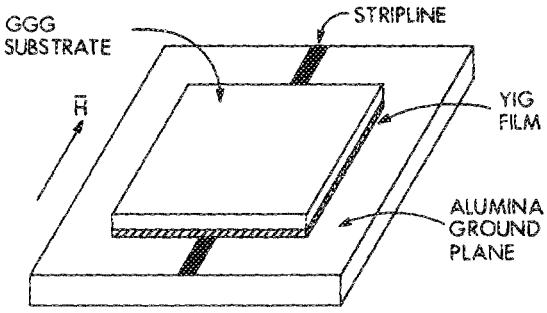

FIG. 2. Schematic diagram of the magnetostatic wave signal-to-noise enhancer device, showing the yttrium iron garnet (YIG) film, the gadolinium gallium garnet (GGG) substrate, the stripline, and the alumina ground plane. The applied field $\bar{H}$ is parallel to the stripline.

Downloaded 26 Dec 2001 to 129.82.140.114. Redistribution subject to AIP license or copyright, see http://ojps.aip.org/japo/japcr.jsp

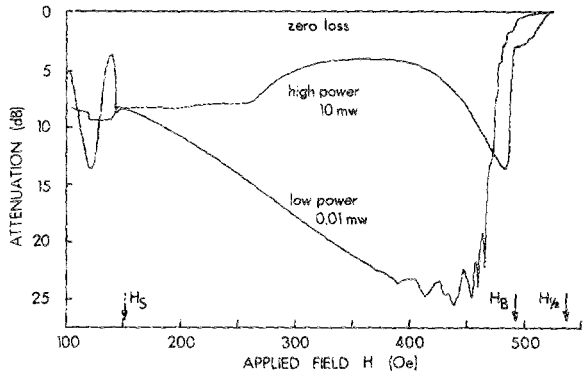

FIG. 3. Transmission loss vs field data for the signal-to-noise enhancer device under low and high input power conditions and an excitation frequency of 3 GHz. The surface wave band edges for zero and large wavenumber MSSW excitations at 3 GHz are indicated by the arrows labeled H_B and H_S, respectively. The arrow labeled $H_{1/2}$ denotes the cutoff field for bulk spin waves at 1.5 GHz. These field parameters are listed in Table I.

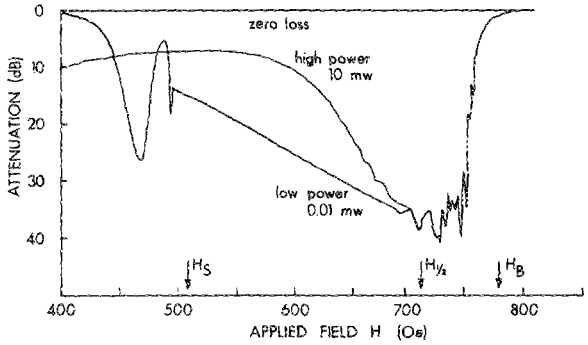

FIG. 4. Transmission loss vs field data for the signal-to-noise enhancer device under low and high input power conditions and an excitation frequency of 4 GHz. The surface wave band edges for zero and large wavenumber MSSW excitations at 4 GHz are indicated by the arrows labeled H_B and H_S, respectively. The arrow labeled $H_{1/2}$ denotes the cutoff field for bulk spin waves at 2 GHz. These field parameters are listed in Table I.

away from the stripline. This results in an *attenuation* of the input power. With increasing input power, the MSSW signal eventually saturates at some critical power level due to the parametric excitation of half-frequency spin waves through the Suhl instability processes.[7] Above this threshold power, therefore, one has a *decrease* in the stripline attenuation factor. With a relatively large attenuation at low powers (below threshold) and a smaller attenuation at high powers (above threshold), one has, in effect, a signal-to-noise enhancer.

Some illustrative data on device attenuation versus field under low- and high-power conditions are shown in Figs. 3 and 4, for fixed frequency operation at 3 and 4 GHz, respectively. These two frequencies were selected to demonstrate explicitly the role of surface magnons and half-frequency parametric magnons in the device operation. The curves in Figs. 3 and 4 will also prove useful for comparison with the BLS data in subsequent sections.

The discussion of the previous section pointed out the various frequency limits for MSSW excitations and bulk spin waves under fixed field conditions. For *fixed frequency operation*, we are interested in the *field* limits for (1) surface magnons at the pump frequency and (2) bulk magnons at one-half the pump frequency. Within the context of Fig. 1 and Eqs. (1)–(5), we see that the entire magnon spectrum will shift up in frequency as the field is increased. We may conveniently denote the low-field limit for which high-k_m MSSW magnons first become available at a given pump frequency as H_S. This H_S is simply the value of the in-plane applied field which satisfies Eq. (4) with f_s equal to the external signal frequency f and $k_m = \infty$ [or the equivalent condition $f_s = f_S$ in Eq. (5)]. In a corresponding manner, we denote the high-field limit for MSSW magnons at the pump frequency as H_B. For an applied field equal to H_B, the bias is such that the frequency point f_B in Fig. 1 coincides with the pump frequency f and the corresponding MSSW magnons satisfy $k_m = 0$ under such conditions. For use in connection with the discussion of Figs. 3 and 4 which follows, and for later use with the BLS discussion, these two MSSW field limits are listed in Table I for both frequencies of interest here (the $H_{1/2}$ parameter in Table I will be considered shortly). All field values in Table I were calculated with $4\pi M_s = 1.84$ kG and $\gamma = 2.8$ GHz/kOe, as obtained from ferromagnetic resonance.

Returning to the data in Figs. 3 and 4, we see a large low-power stripline attenuation over a field range corresponding to H_S–H_B. The values of H_S and H_B from Table I are indicated by appropriately labeled arrows in the figures. The correlation between increased attenuation and the generation and propagation of MSSW excitations away from the stripline is clear. There are more complicated aspects of the device physics than simple cutoff, as evident from the extra structure in the curves of Figs. 3 and 4. These details, however, are not central to the basic results of this paper. (They are important for proper device operation and the BLS technique is a potentially useful tool for the diagnosis of such structure origins.)

The signal-to-noise enhancement function is related to the generation of half-frequency spin waves. Such spin waves may be supported at any field below an upper limit cutoff value $H_{1/2}$ for which f_H is at one-half the pump frequency:

$$f_H(H_{1/2}) = \gamma H_{1/2} = f/2 . \tag{6}$$

Values of $H_{1/2}$ for 3 and 4 GHz are given in Table I. Note that at 3 GHz, the $H_{1/2}$ cutoff is *above* the upper MSSW field limit H_B. This means that (1) half-frequency spin waves are available over the entire range of fields for which the MSSW signals can be generated and (2) the signal-to-noise enhancement at high power should also occur over that entire field range. The realization of these properties is evident by the 10-mW high-power trace in Fig. 3. The stripline attenuation is lower than under low power conditions (the 0.01 mW trace) over the entire field interval H_S–H_B.

TABLE I. Cutoff fields for the magnetostatic surface waves and bulk half-frequency spin waves for the in-plane magnetized YIG film.

Operating frequency	3 GHz	4 GHz
Low-field MSSW cutoff H_S	151 Oe	509 Oe
High-field MSSW cutoff H_B	492 Oe	779 Oe
Half-frequency magnon cutoff $H_{1/2}$	536 Oe	714 Oe

Downloaded 26 Dec 2001 to 129.82.140.114. Redistribution subject to AIP license or copyright, see http://ojps.aip.org/japo/japcr.jsp

The half-frequency magnon situation is a bit different at 4 GHz. In this case, the field limit $H_{1/2}$ falls *below* H_B. This means that the signal-to-noise enhancement should occur only over the field range H_S–$H_{1/2}$, *not* over the entire MSSW range. The high-power attenuation curve in Fig. 4 for 4 GHz confirms the above scenario. The high-power attenuation is lower than the low-power attenuation only below $H_{1/2}$. For fields above $H_{1/2}$, the low- and high-power attenuation traces are virtually identical.

The above results provide a clear demonstration of the signal-to-noise enhancer function and the crucial tie-in with the available spectrum of magnetic excitations. They also illustrate the strengths and weaknesses of simple microwave measurements for MSW device characterization. It is clear that the attenuation characteristics of the device are related to the generation of surface waves under low-power conditions, while the reduced attenuation at high power is due to the parametric generation of half-frequency magnons. The key elements for the device, however, the MSSW and the half-frequency spin wave excitations, are not directly accessible by such measurements. One has no direct, precise measurement capability for the actual waves which are generated in the structure, and no information on the dispersion or energy flow profiles for these waves. Brillouin light scattering provides one useful tool for precisely this kind of measurement. Details of the technique as applied to the signal-to-noise enhancer device are described in the next and subsequent sections.

IV. EXPERIMENT

The Brillouin light scattering technique involves the interaction of an incident photon of frequency $f_{\rm inc}$ and wave vector $\bar{k}_{\rm inc}$ with some long-range excitation in the material (such as a MSW magnon or spin wave) of frequency f_m and wave vector $\bar{k}_m$ to produce a scattered photon of frequency $f_{\rm sc}$ and wave vector $\bar{k}_{\rm sc}$. For this scattering process, both momentum and energy conservation are required:

$$\bar{k}_{\rm sc} = \bar{k}_{\rm inc} \pm \bar{k}_m \,, \tag{7a}$$

$$f_{\rm sc} = f_{\rm inc} \pm f_m \,. \tag{7b}$$

The ($\pm$) signs correspond to the destruction of an existing magnon or the creation of a new magnon, respectively. It is necessary to have an appropriate scattering geometry which can satisfy Eq. (7a) for the desired range of $\bar{k}_m$ values of interest, and to have a suitable instrument to detect the small shift of $\pm f_m$ in frequency for the scattered light. The scattering geometry, then, defines the $\bar{k}_m$ value (or range of values) which is accessed in the experiment. The interferometer measurement yields the frequency shift for the magnon(s) under study. The strength of the scattered light at $f_{\rm sc}$ is a measure of the magnon amplitude in the region of the sample probed by the laser beam light source, with a spot size typically on the order of 10–50 μm. The f_m and $\bar{k}_m$ data yield a direct measurement of the magnon dispersion. It is important to note at this point that the actual scattering measurement is not trivial. Magnon-photon scattering is generally a weak process and the frequency shifts of interest here, on the order of GHz, are down by more than a factor of 10^6 from the incident light frequency.

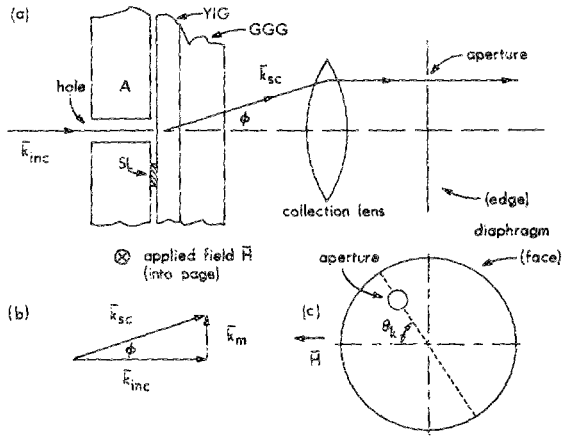

FIG. 5. Schematic diagram of the light scattering geometry for the Brillouin light scattering detection of magnetostatic wave excitations in the signal-to-noise enhancer device structure. (a) shows the incident and scattered light beams (labeled by wave vectors $\bar{k}_{\rm inc}$ and $\bar{k}_{\rm sc}$, respectively), a cross-section schematic view of the device [with the alumina ground plane (A), the stripline (SL), the yttrium iron garnet film (YIG), and the gadolinium gallium garnet substrate (GGG)], and the collection optics (lens and aperture diaphragm). (b) shows the wave vector addition algebra for the incident light ($\bar{k}_{\rm inc}$) and the stripline generated surface magnon ($\bar{k}_m$) to yield the appropriate scattered light at $\bar{k}_{\rm sc}$. (c) shows a front view of the aperture diaphragm. The parameter θ_k represents the spin wave propagation angle with respect to the applied field and ϕ is the angle between the scattered light collected for analysis and the axis of the collection lens.

In the present context, one is interested in probing MSSW excitations with in-plane magnon wave vectors. One would also like to select particular $\bar{k}_m$ values, both in magnitude and direction, relative to the in-plane field. For the range of $|\bar{k}_m|$ values of interest in YIG film devices, 0 –10^4 cm^{-1}, a forward scattering configuration as shown in Fig. 5 is needed. Figure 5(a) details the scattering setup, Fig. 5(b) diagrams the wave vector algebra for the destruction of an in-plane magnetic excitation of wave vector $\bar{k}_m$, and Fig. 5(c) shows a forward view of one type of collection optics aperture for wave vector selection.

Consider the scattering setup of Fig. 5(a). The sample is accessed through a small hole in the alumina ground plane of the device (labeled "A"). The incident light of wave vector $\bar{k}_{\rm inc}$ passes through the hole and interacts with the excitations present in the YIG film. This access hole must be strategically located at an appropriate distance from the stripline [shown in cross section in Fig. 5(a) and labeled "SL"] to sample the magnetic excitations which are generated by and propagate away from the stripline. If the hole is too close, the excitation situation becomes too complicated for simple analysis; if it is too far away, the magnon signals are too weak to give any measurable scattering. Since the stripline is deposited on the alumina ground plane in this device, it is necessary to choose a hole position and drill quite accurately at that position in order to have a workable situation for the light scattering experiment. For the present results, the hole size was about 1 mm and the hole–stripline distance was also 1 mm. The hole was positioned 3 mm from the edge of the GGG substrate. The laser beam diameter was less than 100 μm. The incident laser power at the film was kept below 10 mW or so to avoid heating problems.

Downloaded 26 Dec 2001 to 129.82.140.114. Redistribution subject to AIP license or copyright, see http://ojps.aip.org/japo/japcr.jsp

The collection lens and diaphragm in Fig. 5(a) serve to collimate the scattered light and select the particular wave vector (or range of wave vectors) for that portion of the scattered light which is to be analyzed. Scattered light from magnons with specific $\bar{k}_m$ values can be selected for frequency analysis by placing an aperture at an appropriate position on the diaphragm.[9] The in-plane $\bar{k}_m$ direction relative to the field is controlled by the aperture orientation, as indicated in Fig. 5(c), where θ_k is the angle between $\bar{k}_m$ and $\bar{H}$.

The minimum selectable magnon wave number is zero, corresponding to an aperture precisely on axis. The maximum accessible value of k_m corresponds to an aperture location at the perimeter of the active collection lens area. For the f1.4, 50-mm focal length lens used in this work, the maximum accessible k_m value was about 4×10^4 cm^{-1}. For the experiments for which specific $\bar{k}_m$ values were critical to the measurement, an aperture size of 50 μm was used. Limiting the collected light to such a small aperture, however, severely reduces the scattered light signal available for frequency analysis. For many cases, data collection with *no* aperture in place is entirely adequate. In such instances, the scattered light contains information on the *entire* range of accessible magnon wave vectors, $0<\theta_k<360°$ and $k_m<4\times10^4$ cm^{-1}. A slit-type aperture was used in some cases to select specific θ_k values (in-plane propagation direction) only.

The overall system layout is shown schematically in Fig. 6. The argon laser was used in a stabilized, single mode configuration on the 5145-Å green line. Various mirrors and a focusing lens were used to direct the laser beam on the sample for forward scattering. A quarter-wave plate was used to obtain an appropriate linearly polarized incident beam. Proper focusing of the two lenses required a two-step procedure. A backscattering configuration was first used (dotted line in Fig. 6) to adjust the collection lens. The system was then switched to the forward scattering configuration for adjustment of the incident beam focusing lens. The scattered light was analyzed by a multipass tandem Fabry–Perot interferometer (FPI) following the design of Sandercock.[10] The present system has high contrast, in excess of 10^{12}, and a finesse of approximately 50. The photon counting system uses a high-sensitivity, low dark count photomultiplier tube (PMT). Data were collected with a standard multichannel analyzer (MCA). It is important to emphasize once more that for this work, the scattering is weak and the frequency shifts are small. The high-sensitivity Fabry–Perot interferometer was crucial to the success of the measurements.

The in-plane magnetic field was provided by a Helmholtz pair with a coil separation of 8 cm. The maximum field was 2.5 kOe, and the field homogeneity over the YIG film was better than 1%. The microwave power was provided by a standard 2– 4 GHz sweep oscillator with a maximum output power of 40 mW. Input power levels were controlled by a precision attenuator. Power levels cited herein were measured at the input port of the device under test. Data were obtained for input powers from 0.05 to 40 mW. The output port of the device was terminated with a matched load.

The overall measurement involves the setting up of a properly focused and aligned optical system, the application of appropriate microwave power to the device, and frequency analysis of the scattered light. As discussed earlier, one would expect to see scattered light at frequency f_{sc} which is shifted from the incident light frequency f_{inc} by $\pm f_m$, where the ($\pm$) sign corresponds to the annihilation or creation of a magnon at frequency f_m which satisfies the appropriate momentum or wave vector conservation constraint.

For purposes of illustration, two sample spectra are shown in Fig. 7. These spectra were obtained at 3 GHz with

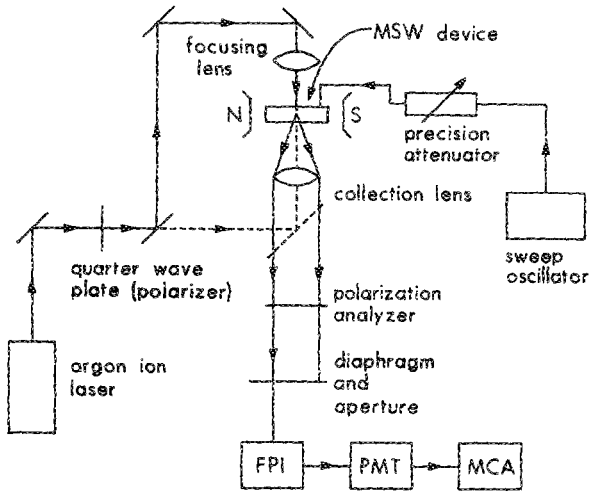

FIG. 6. Block diagram of Brillouin light scattering spectrometer system.

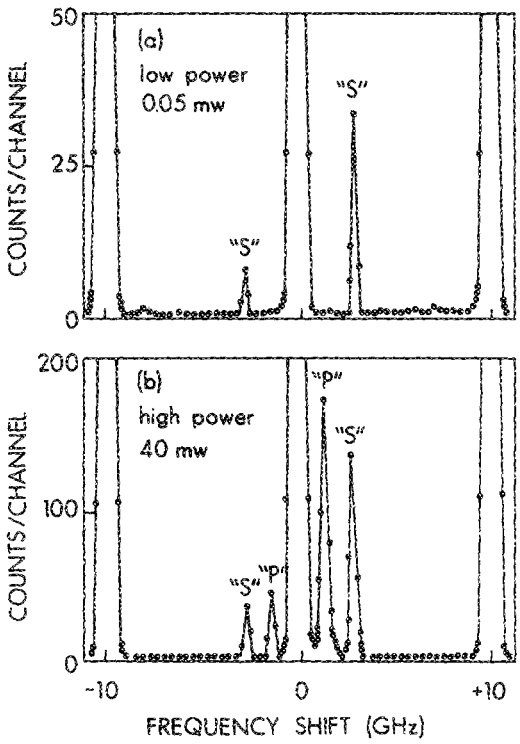

FIG. 7. Typical Brillouin light scattering spectra for the device structure with 3-GHz microwave excitation, an applied field of 400 Oe parallel to the stripline axis, and no aperture diaphragm in the collection optics setup. Spectrum (a) is for relatively low input power of 0.05 mW. Spectrum (b) is for a relatively high input power of 40 mW. The peaks labeled "S" and "P" correspond to the magnetostatic surface waves at the pump frequency and the half-frequency spin waves, respectively.

Downloaded 26 Dec 2001 to 129.82.140.114. Redistribution subject to AIP license or copyright, see http://ojps.aip.org/japo/japcr.jsp

an applied field of 400 Oe parallel to the stripline. Figure 7(a) is for low-power microwave excitation (0.05 mW) at the input port of the device, Fig. 7(b) is for 40-mW input power. These data were obtained with *no* aperture in place. These and similar spectra will be discussed at length in subsequent sections. The essential point here is that the spectra do indeed reveal the presence of excited magnons in the device structure. The "S" peaks in Fig. 7(a) are shifted from the central line by $\pm$ 3 GHz and are due to scattering from the MSSW magnons generated in the device. The additional "P" peaks in Fig. 7(b) are shifted from the central line by $\pm$ 1.5 GHz and are due to scattering from the parametric half-frequency spin waves which are excited above the Suhl threshold.

The central line in the figure at "0" GHz corresponds to Rayleigh scattering at the incident light frequency f_{inc}. This Rayleigh peak is used for electronic stabilization of the FPI system.[10] The additional large satellite peaks at $\pm$ 10 GHz are actually higher- and lower-order Rayleigh signals. These peaks indicate the free spectral range of the Fabry–Perot interferometer. The "S" and "P" signal peaks associated with these Rayleigh side peaks are suppressed for the tandem interferometer. Some elaboration on the nuances of FPI spectra and multipass-tandem Fabry–Perot interferometers in general may be found in Ref. 11.

V. MAGNETOSTATIC SURFACE WAVES

The essential result for light scattering on MSSW excitations, the presence of "S" peaks in the Brillouin spectra, was already shown in Fig. 7. This spectra example was for *no* aperture and *no* $\bar{k}_m$ selection. The interferometer "sees" all accessible magnons which satisfy $k_m < 4\times10^4$ cm^{-1}. This section is concerned with several key aspects of the BLS data on these MSSW excitations, with particular emphasis on the dispersion characteristics of these waves.

In order to measure dispersion characteristics by the BLS technique, it is necessary to obtain spectra with an appropriate selection aperture in place to limit the range of $\bar{k}_m$ values which can contribute to the scattered light for FPI analysis. It is also necessary to set the value of the static field properly so that the excited MSSW magnons at the drive frequency actually correspond to the $\bar{k}_m$ values which have been aperture selected.

The connection between the field selected $\bar{k}_m$ values for perpendicular propagation through the dispersion constraint [Eq. (4)] and the aperture selected $\bar{k}_m$ values for light collection is demonstrated by the intensity versus field data in Fig. 8. Here, the amplitude of the "S" peak is shown as a function of applied field for an input signal frequency of 3 GHz and an on-axis 50-μm aperture. An on-axis aperture restricts the light collection to scattering from magnons which satisfy $\bar{k}_m \cong 0$. From Secs. II and III, we would expect to see a peak in the scattering intensity at the field for which $f_B = 3$ GHz is satisfied, corresponding to the generation of 3 GHz MSSW signals with $\bar{k}_m = 0$. This field is given by the H_B value in Table I for 3 GHz and is also indicated by the arrow in Fig. 8. We see that the observed field for maximum scattering is close to the expected position. The discrepancy is below 10 Oe and is probably related to the uncertainty in the value of $4\pi M_s$ used to calculate H_B and small errors in the measured field.

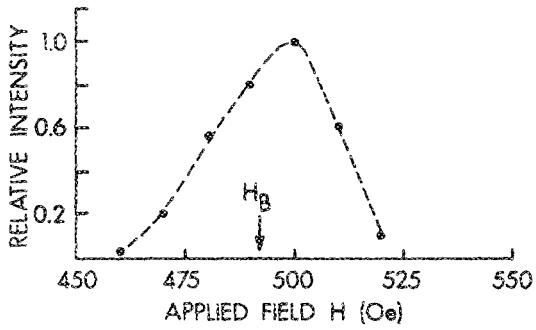

FIG. 8. Brillouin light scattering intensity vs applied field for an "S" peak signal as shown in Fig. 7, but for an on-axis aperture of 50 μm in the diaphragm in the collection optics setup. The field and frequency values were 400 Oe and 3 GHz, respectively, as for Fig. 7. The input power was 0.05 mW for these data.

Just as the position of the "S" peak in field is controlled by the position of the selection aperture, the field *width* of the peak is related to the size of the aperture. For the 50-μm aperture and scattering geometry in use here, the spread in k_m is about 55 cm^{-1}. From Eq. (4) this spread in k_m translates into a spread in field of about 75 Oe, in very good agreement with the intensity versus field profile in Fig. 8.

From data similar to those in Fig. 8, it is possible to use the BLS technique to measure MSSW frequency versus field and/or wave vector. Some representative measurements are

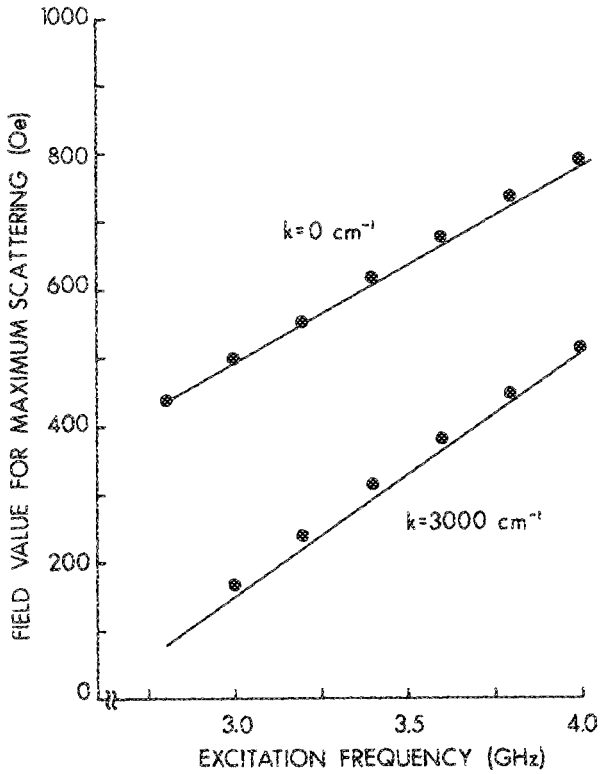

FIG. 9. Field for maximum "S" peak scattering intensity vs frequency for two different 50-μm aperture positions on the diaphragm in the collection optics setup, one on axis, corresponding to a $\bar{k}_m$ value of zero (as in Fig. 8), and one slightly off axis, corresponding to perpendicular propagation and $k_m = 3000$ cm^{-1}. The solid lines are based on MSSW theory.

Downloaded 26 Dec 2001 to 129.82.140.114. Redistribution subject to AIP license or copyright, see http://ojps.aip.org/japo/japcr.jsp

shown in Fig. 9 for two specific aperture selected $\bar{k}_m$ values. Each data point represents the peak scattering intensity in an intensity versus field profile (as in Fig. 8) for each of the indicated frequencies. The upper set of points is for $\bar{k}_m = 0$. The lower set of points is for an off-axis aperture position corresponding to $k_m = 3000\ \text{cm}^{-1}$ and $\theta_k = 90°$ (MSSW propagation perpendicular to the field and stripline direction). The 3000 cm^{-1} value for k_m was selected by displacing the diaphragm aperture off axis by an angle of 1.5° [the angle ϕ in Fig. 5(a)]. By rotating the aperture around the scattering axis, it was possible to verify experimentally that the MSSW in-plane propagation angle θ_k was in fact $90 \pm 5°$. The solid lines in the figure were calculated from Eq. (4) with appropriate parameters for the YIG film under test, $d = 26.6\,\mu\text{m}$, $4\pi M_s = 1.84$ kG, and $\gamma = 2.8$ GHz/kOe. The agreement between the data and the theoretical curves is quite reasonable. As was the case for the peak position in Fig. 8, the small discrepancy which does appear can probably be attributed to some uncertainty in $4\pi M_s$ and/or H.

The final point of discussion for this section concerns the relative magnitudes of the "S" peaks on either side of the Rayleigh peak in Figs. 7(a) and 7(b). In previous studies of thermally excited MSSW excitations, the different intensities for the upshifted and downshifted peaks have been related to the nonreciprocal propagation characteristics of the surface modes (discussed briefly in Sec. II) and scattering cross section considerations for the creation versus the destruction of a magnon.[12] In the present circumstances, the very strong "S" peaks on *both* sides of the central Rayleigh line represent something of an anomaly. Since the very strong scattering which is observed should only come from the destruction of MSSW magnons which were *excited* by the stripline power in the first place, one would expect to see *only* an upshifted "S" peak. Any downshifted peak would correspond to MSSW magnons which are created in the scattering process itself. Such scattering should be very weak and essentially unresolved on the scale of Fig. 7(a) or 7(b).

VI. HALF-FREQUENCY PARAMETRIC MAGNONS

Turn now to the "P" magnons which appear in the BLS spectra for high power stripline excitation and appropriate field values for half-frequency spin waves. The presence of such parametric magnons is implicit from the device attenuation data of Sec. III. Figure 7(b), moreover, provides explicit proof that half-frequency parametric magnons are generated at high power. The next section of this paper will present data on the "S" and "P" magnon scattering intensity versus field, essentially BLS analogs of the attenuation curves of Figs. 3 and 4. The purpose of this section is to describe some of the important "P" magnon characteristics and relate those characteristics to theory.

It is important to recall that the "P" magnons are really a manifestation of the spin wave instability effects initially explained by Suhl.[7] In fact, the threshold microwave power level for "P" magnon generation as a function of static field resembles a so-called "butterfly" curve for subsidiary absorption. Butterfly curves derived from microwave data for single-crystal YIG materials have been discussed recently by Patton and Jantz.[13] Some basic BLS butterfly curve results

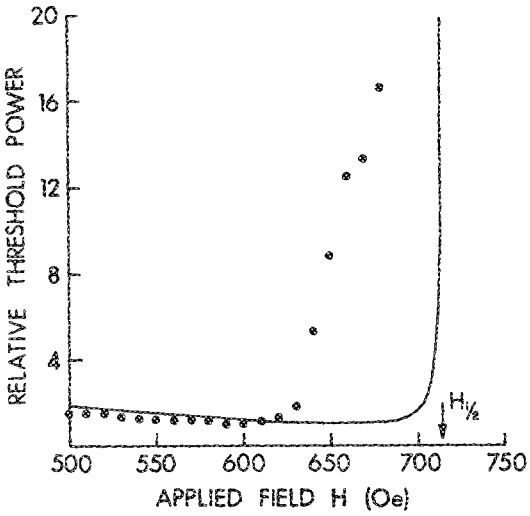

FIG. 10. Instability threshold power for "P" magnon generation as a function of the static applied field for an operating frequency of 4 GHz and no aperture in the collection optics setup. The data are normalized to the minimum threshold value at $H = 600$ Oe. The solid line corresponds to the "butterfly curve" from theory.

for YIG films have also been reported by Wettling *et al.*[14] and Wilber.[15] Detailed results on the spin wave instability and butterfly curve characteristics for magnetostatic waves in device structures will appear as a separate publication.

Measured values of the input power threshold for the generation of "P" magnons as a function of static field for 4-GHz excitation are shown in Fig. 10. The data are normalized to the minimum threshold value. The actual minimum threshold input power level at 4 GHz was approximately 0.2 mW. The data in Fig. 10 have the general appearance of a butterfly curve, with the gradual decrease in threshold to a minimum value at some field approximately midband for low wavenumber half-frequency spin waves (that is, $f_H < f/2 < f_B$), followed by a more rapid increase in threshold at higher fields. As the static field approaches the cutoff field for half-frequency spin waves, $H_{1/2}$, the threshold becomes too large to measure. (The theoretical threshold becomes infinite at $H = H_{1/2}$.)

The solid line in the figure represents the theoretical threshold power versus field based on the Suhl theory as modified for a uniform in-plane microwave pump field perpendicular to the (in-plane) static field in a thin film.[16] This particular form of the theory does not take into account the MSSW character of the pumped mode, the magnetostatic nature of the parametric magnons, or the wave vector dependence of the spin wave linewidth. The lack of quantitative agreement between the data and the theory for fields between the experimental butterfly curve minimum and $H_{1/2}$ is probably related to these theoretical oversimplifications. Wettling *et al.*[14] and Wilber[15] have shown that the parametric magnons which are generated in YIG films at 10 GHz under parallel pumping or subsidiary absorption, for example, are magnetostatic in character.

One important aspect of the "P" magnons concerns the wave vector direction and magnitude for the excited modes. As discussed above, the use of selective apertures in the BLS experiment allows one to experimentally determine these pa-

Downloaded 26 Dec 2001 to 129.82.140.114. Redistribution subject to AIP license or copyright, see http://ojps.aip.org/japo/japcr.jsp

rameters. Such data reveal that the "P" magnon in-plane wave vector components are *parallel* to the stripline and static field direction, in good agreement with the theoretical predictions from Ref. 16. The in-plane component of the "P" magnon wave vector is on the order of 10^3–10^4 cm^{-1}, which is the expected range for MSW excitations in 26-μm-thick films. As mentioned above, a detailed description of the BLS results on spin wave instability effects in MSW device structures will be published separately.

VII. INTENSITY PROFILES

The last section of this paper is concerned with intensity profiles of scattering signal versus field for the various BLS magnon peaks discussed earlier. We will explicitly consider such profiles for the "S" peaks under low and high power conditions and the "P" magnons which are generated under high power conditions only. Results are presented for the two frequencies which were emphasized in the previous sections, 3 and 4 GHz. To some extent, such profiles are simply analogs of the attenuation versus field curves of Figs. 3 and 4. Since the BLS profiles can focus in on specific magnetic excitations, however, such data can provide much more insight into the actual device physics than attenuation curves.

Some representative BLS profile data are shown in Figs. 11 and 12 for 3 and 4 GHz, respectively. These profiles were obtained by monitoring the scattering intensity for the particular BLS peak of interest, e.g., one of the "S" or "P" peaks in Fig. 7, as the static field was varied. For the profiles under low-power conditions [Figs. 11(a) and 12(a)], the relatively weak scattering signals made it necessary to obtain data point by point. For the high-power profiles [Figs. 11(b), 11(c), 12(b), and 12(c)], it was possible to use the continuous scanning technique described in Ref. 9. All data were obtained with no selection aperture in the collection optics setup; all $\bar{k}_m$ values accessible to the collection lens were monitored.

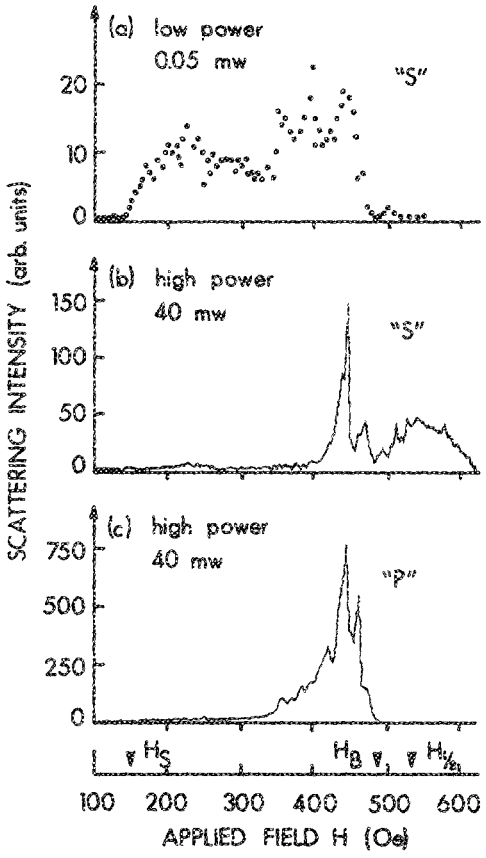

FIG. 11. Profiles of the BLS scattering intensity vs applied static field H for an operating frequency of 3 GHz and no collection optics aperture. Profile (a) is for an "S" magnon peak and relatively low input power (0.05 mW) such that no "P" magnons are generated. Profiles (b) and (c) are for the "S" and "P" magnon peaks, respectively, but with maximum input power (40 mW). The cutoff field parameters H_S, H_B, and $H_{1/2}$ correspond to various band limits for "S" and "P" magnons and are listed in Table I.

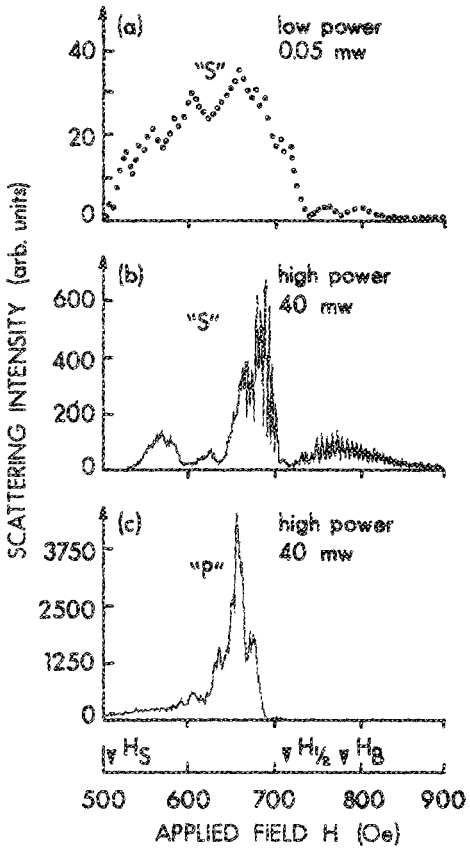

FIG. 12. Profiles of the BLS scattering intensity vs applied static field H for an operating frequency of 4 GHz and no collection optics aperture. Profile (a) is for an "S" magnon peak and relatively low input power (0.05 mW) such that no "P" magnons are generated. Profiles (b) and (c) are for the "S" and "P" magnon peaks, respectively, but with maximum input power (40 mW). The cutoff field parameters H_S, H_B, and $H_{1/2}$ correspond to various band limits for "S" and "P" magnons and are listed in Table I.

First consider the 3-GHz profile data in Fig. 11. Figure 11(a) shows the "S" magnon BLS intensity for a low input power, well below the level needed for the generation of "P" magnons. Due to the low power, the scattering levels were rather weak, and the point-by-point data do show some scatter. Recall that MSSW signals can be supported over a field range from H_S to H_B. These fields (along with $H_{1/2}$) are indicated by arrows along the field axes in all segments of Fig. 11 (and Fig. 12). The wavenumber of the MSSW signal ranges from some large value for fields approaching H_S to approximately zero at $H = H_B$. The data show that the low-power "S" magnon scattering intensity is quite strong over the field interval from H_S to H_B and essentially zero outside

Downloaded 26 Dec 2001 to 129.82.140.114. Redistribution subject to AIP license or copyright, see http://ojps.aip.org/japo/japcr.jsp

this region. The complicated structure in the profile of Fig. 11(a) may be related to the more efficient generation of MSSW signals at particular wavelengths by the stripline. The small peak slightly above H_B may be connected with evanescent wave effects to be discussed shortly.

"S" and "P" magnon profiles for high input power at 3 GHz are shown in Figs. 11(b) and 11(c), respectively. The power level here is 40 mW, much higher than the 10-mW level for the companion microwave data in Fig. 3. The main point here is that the high power leads to a drastic change in the "S" magnon profile and gives rise to strong "P" magnon scattering which tracks, more or less, the high-power "S" magnon response. Although a detailed series of measurements on the "S" and "P" magnon profiles as a function of power has not been made, these BLS results do confirm rather directly the magnon scenario developed for the device in previous sections.

One very interesting aspect of the magnon profiles in Fig. 11 concerns the appreciable scattering for fields *above* H_B. MSSW excitations of the Damon–Eshbach genre are not supported in the YIG film for $H > H_B$. These signals are tentatively attributed to "evanescent" or nonpropagating surface waves. We will comment further on these waves in connection with Fig. 12.

Profile data for 4-GHz stripline excitation are shown in Fig. 12. Recall that for 4 GHz, the cutoff field for half-frequency spin waves falls *below* H_B, as indicated by the arrows in the figure. Except for this difference, we have the same general situation as for 3 GHz. The pronounced "S" magnon profile over the allowed MSSW field interval at low power (H_S–H_B) gives way to a much different profile at high power. The intensity profile for the "P" magnons, which come in at high power, shows a sharp cutoff at $H_{1/2}$.

The low-power "S" magnon profiles at 4 GHz do not show the same pronounced cutoff at $H = H_B$ as at 3 GHz. The main region for strong "S" magnon scattering in Fig. 12(a) stops at a field 50 Oe below H_B. As at 3 GHz, the structure in the low power "S" magnon profile between H_S and H_B is probably related to the changes in stripline coupling at the different MSSW wavelengths.

The 4-GHz "S" magnon profiles also show a significant amount of scattering for fields above H_B. The signals are tentatively attributed to evanescent surface waves. Such waves may be generated by the stripline with a ground plane in close proximity, as in this device. They are nonpropagating and carry no power. Hence, such waves are not evident from microwave attenuation measurements. Some "S" magnon signal above H_B is also apparent at high power, as in Fig. 12(b). The entire "S" magnon "tail" in Fig. 12(b) is rather fascinating. This tail starts at $H = H_{1/2}$, peaks at some field near H_B and decreases in intensity at higher fields. The tail shows a peculiar periodic structure which may be related to some kind of interference between the propagating MSSW signals and the evanescent waves. A detailed study of the evanescent modes is presently in progress.

VIII. SUMMARY AND CONCLUSION

The results presented here demonstrate the utility of the BLS technique for magnetostatic wave device characterization. The results are of both fundamental and practical importance. One is able to detect and characterize the basic magnetic excitations *in situ* in the device. The technique is very sensitive and the magnon scattering signals are quite strong. In addition, parametric spin waves which are excited in the device above some critical power can be easily and unambiguously detected. The BLS technique, therefore, is ideal for probing directly the parametric, nonlinear magnon processes which occur in such devices.

ACKNOWLEDGMENTS

The authors are grateful to Dr. J. D. Adam, Westinghouse Research and Development Center, Pittsburgh, for providing the magnetostatic wave device used in these experiments. This work was supported by the U.S. Air Force, Contract No. F-19628-85-K-0002.

[1] J. C. Sethares, in *Proceedings of the 1981 Rome Air Development Center Microwave Magnetics Technology Workshop*, Hanscom, Massachusetts, June 10–11, 1981, Report no. RADC-TR-83-15, Jan. 1983.
[2] R. W. Damon and J. R. Eshbach, J. Phys. Chem. Solids **19**, 308 (1961).
[3] G. Srinivasan and C. E. Patton, IEEE Trans. Magn. **MAG-21**, 1797 (1985).
[4] G. Srinivasan and C. E. Patton, Appl. Phys. Lett. **47**, 761 (1985).
[5] J. D. Adam, IEEE Trans. Magn. **MAG-16**, 1068 (1980).
[6] J. D. Adam and S. N. Stitzer, Appl. Phys. Lett. **36**, 485 (1980).
[7] H. J. Suhl, J. Phys. Chem. Solids **1**, 209 (1957).
[8] J. R. Sandercock and W. Wettling, J. Appl. Phys. **50**, 7784 (1979).
[9] W. D. Wilber, W. Wettling, P. Kabos, C. E. Patton, and W. Jantz, J. Appl. Phys. **55**, 2533 (1984).
[10] J. R. Sandercock, Top. Appl. Phys. **51**, 173 (1982).
[11] C. E. Patton, Phys. Repts. **103**, 251 (1984).
[12] R. E. Camley, P. Grunberg, and C. M. Mayer, Phys. Rev. B **26**, 2609 (1982).
[13] C. E. Patton and W. Jantz, J. Appl. Phys. **50**, 7082 (1979).
[14] W. Wettling, W. D. Wilber, P. Kabos, and C. E. Patton, Phys. Rev. Lett. **51**, 1680 (1983).
[15] W. D. Wilber, Ph.D. dissertation, Colorado State University, Fort Collins, CO, 1986 (unpublished).
[16] C. E. Patton, J. Appl. Phys. **40**, 2837 (1969).

Downloaded 26 Dec 2001 to 129.82.140.114. Redistribution subject to AIP license or copyright, see http://ojps.aip.org/japo/japcr.jsp